


## Original Article

## Sirt1 blocks nucleus pulposus and macrophages crosstalk by inhibiting RelA/Lipocalin 2 axis



Yi-Fan Wei<sup>a,1</sup>, He-Long Zhang<sup>a,1</sup>, Ling-Zhi Li<sup>a,1</sup>, You Lv<sup>b,1</sup>, He Li<sup>c</sup>, Zhi Li<sup>d</sup>, Feng-Lei Yu<sup>e</sup>,  
Tao Jiang<sup>a</sup>, Tian-You Zhang<sup>a</sup>, Feng Xin<sup>f,\*</sup>, Cheng Ma<sup>a,\*\*</sup>, Yong-Xin Ren<sup>a,\*</sup> 

<sup>a</sup> Department of Orthopaedics, The First Affiliated Hospital of Nanjing Medical University, 300 Guangzhou Rd, Nanjing, 210029, China

<sup>b</sup> Department of Orthopaedics, Lianyungang Clinical College of Nanjing Medical University, 6 Zhenhua East Rd, Lianyungang, 221000, China

<sup>c</sup> Department of Sports Medicine, Lianyungang Clinical College of Nanjing Medical University, 6 Zhenhua East Rd, Lianyungang, 221000, China

<sup>d</sup> Department of Orthopaedics, Geriatric Hospital of Nanjing Medical University, 65 Jiangsu Rd, Nanjing, 210024, China

<sup>e</sup> Department of Trauma and Orthopaedics, The First People's Hospital of Kunshan, 566 East Qianjin Rd, Suzhou, 215000, China

<sup>f</sup> Department of Orthopaedics, Xuzhou Cancer Hospital, 131 Huancheng Rd, Xuzhou, 221005, China

## ARTICLE INFO

## Keywords:

Intervertebral disc degeneration

Lipocalin 2

Macrophage

NF-κB

Sirt1

## ABSTRACT

**Background:** Intervertebral disc degeneration (IVDD) stands as a primary pathophysiological driver of low back pain, yet no therapeutic intervention effectively arrests its progression. Evidence shows that certain Sirt1 agonists may confer protective effects on intervertebral discs, but the underlying mechanisms remain unclear. This study aims to delineate the interaction between Sirt1 and the inflammatory microenvironment, offering potential novel avenues for IVDD prevention and treatment.

**Methods:** *In vitro* IL-1β-induced nucleus pulposus cells (NPCs) degenerative model and *in vivo* a mouse annulus fibrosus needle puncture model in Sirt1 transgenic (Sirt1<sup>TG</sup>) and the same litter WT mice were used to investigate the role of Sirt1 in homeostasis and inflammation. Mechanistic insights were obtained through RNA sequencing, co-immunoprecipitation (Co-IP), luciferase assays, and chromatin immunoprecipitation-(ChIP)-PCR. A co-culture system of Raw264.7 and NPCs was employed to assess the involvement of Lipocalin 2.

**Results:** Our study demonstrated reduced Sirt1 expression in degenerating human nucleus pulposus (NP) tissue. Both *in vitro* and *in vivo* data revealed that NP-specific overexpression of Sirt1 inhibited extracellular matrix degradation and inflammation. Mechanistically, Sirt1 suppressed the acetylation of RelA/p65 at lysine 310 and phosphorylation at serine 536, with the C-terminus of Sirt1 and the RHD-NLS domain of RelA mediating to their interaction. Furthermore, NPCs-derived Lipocalin 2 was identified as a cytokine involved in macrophage chemotaxis and M1 polarization to exacerbate inflammation.

**Conclusion:** Our work revealed that Sirt1 negatively regulates Lipocalin 2, thereby ameliorating the inflammatory milieu and blocking NPCs and macrophages crosstalk.

**The Translational Potential of this Article:** This study illuminates the crucial role and molecular mechanisms of Sirt1 in regulating the NP microenvironment. These insights shed light on strategies for the prevention and treatment of IVDD-related herniation and low back pain. By pinpointing specific biological targets, the screening of smallmolecule compounds with significant clinical implications can be facilitated. This translational innovation promises to optimize cells communication within intervertebral disc microenvironment via localized drug delivery, potentially improving patient outcomes and satisfaction following spinal fusion or discectomy surgeries.

\* Corresponding author.

\*\* Corresponding author.

\*\*\* Corresponding author.

E-mail addresses: [925866554@qq.com](mailto:925866554@qq.com) (F. Xin), [cheng15787531@163.com](mailto:cheng15787531@163.com) (C. Ma), [renyongxinjsph@163.com](mailto:renyongxinjsph@163.com) (Y.-X. Ren).

<sup>1</sup> These authors contributed equally to this work.

## 1. Introduction

Low back pain (LBP) is a major cause of disability worldwide and imposes a heavy burden on the health care system [1] and its incidence is closely correlated with the severity of degeneration of intervertebral discs (IVDs) [2]. Nucleus pulposus cells (NPCs), the primary cellular constituents of the NP, play a pivotal role in extracellular matrix (ECM) synthesis, and their dysfunction is implicated in the pathogenesis of intervertebral disc degeneration (IVDD). This process is thought to be driven by the aberrant secretion of pro-inflammatory molecules by NPCs, as well as immune cells such as macrophages and lymphocytes [3, 4]. These secreted cytokines trigger a cascade of pathogenic responses, including autophagy, senescence, and apoptosis within IVD tissue [5–8], processes that may be pivotal targets for developing innovative therapeutic strategies.

Sirt1 holds a prominent position among the sirtuin family in mammals, classified as a class III histone deacetylase. It shares homology with *Sir2*, a key regulator of yeast longevity that modulates cellular silencers. Sirt1 is a nicotinamide adenosine dinucleotide (NAD<sup>+</sup>)-dependent deacetylase that can be used to deacetylate not only histones but also some non-histone proteins, such as p53 [9], Foxo [10], NF-κB [11], and PPAR-γ [12]. Previous studies have demonstrated that Sirt1 expression is markedly reduced in aged and degenerated human IVDs [13–15]. However, the detailed mechanisms through which Sirt1 exerts its protective effects, particularly its interaction with inflammatory pathways like NF-κB, remain unclear.

The NF-κB pathway is a crucial modulator of numerous cytokines, adhesion molecules, and matrix-degrading enzymes within IVD [16]. Yet, the precise downstream targets, particularly within the context of chronic disc inflammation, are not fully elucidated.

Recent attention has shifted toward Lipocalin 2 (Lcn2), also known as neutrophil gelatinase-associated lipocalin (NGAL) in humans, a protein originally identified in neutrophils but now recognized for its role in various cell types, including macrophages, hepatocytes, epithelial cells, adipocytes, and osteoblasts [17,18]. Its ability to induce pro-inflammatory cytokines, such as inducible nitric oxide synthase (iNOS), suggests a potential role in exacerbating secondary damage and impeding locomotor recovery after spinal cord injury [19]. Here, RNA sequencing analysis has uncovered that Lcn2 gene expression is inversely proportional to Sirt1 in NPCs, which may reveal the potential target for Sirt1 to have an anti-inflammatory effect in IVDD. Nonetheless, the direct involvement of Lcn2 in IVDD acceleration and the detailed mechanisms require further investigation.

In this study, we elucidated that Sirt1 expression is diminished in degenerative human NP tissue, and that specific overexpression of Sirt1 can effectively suppress p65 acetylation and its transcriptional activity. By single-cell RNA sequencing (scRNA-seq) datasets and bulk RNA sequencing, we seek to explore the cellular heterogeneity of NPCs and identify key molecular pathways involved in IVDD. Our findings suggest that Sirt1 exerts anti-inflammatory effects by suppressing Lcn2, which in turn limits macrophages recruitment and M1 polarization. This work sheds light on new ideas and the underlying mechanisms of cellular therapy for IVDD with a view to further clinical translational studies.

## 2. Materials and methods

### 2.1. Human NP sample collection

A total of 20 patients who received discectomies for lumbar disc herniation were included in this study at The First Affiliated Hospital of Nanjing Medical University (2018 SR-233), with an age distribution of 21–82 years, excluding spinal tuberculosis and scoliosis (Supplement Table S2). Informed consent was obtained from patients before all specimens were obtained. All patients had preoperative magnetic resonance imaging (MRI) and the degree of intervertebral disc degeneration was assessed using the modified Pfirrmann classification [20], where

Grade 2 to Grade 4 were defined as Mild Degeneration and Grade 5 to Grade 8 were defined as Severe Degeneration. All samples were placed in 4 % paraformaldehyde immediately after excision and replaced with fresh phosphate buffer saline after 24 h for preservation at 4 °C.

### 2.2. Cell culture and transfection of plasmids

NPCs were isolated from the NP tissue of C57BL/6 mice (4-week-old) with sterile sharp surgical blades and digested at 37 °C overnight with 0.25 % trypsin (Gibco, USA) and 0.2 % collagenase II (Sigma, USA) and then suspended in DMEM/F12 medium containing 10 % fetal bovine serum (Thermo, USA). Passages were conducted after cell fusion and the first four passages of cells were used for subsequent experiments.

Primary NPCs were stimulated with 20 ng/mL IL-1β to establish a degeneration model, treated with 10 μM EX-527 for selectively inhibiting Sirt1 or 1.0 μM Bay11-7082 for suppressing NF-κB signaling pathway, and treated with recombinant mouse Lcn2 (rmLcn2) for exogenous supplementation.

For Sirt1-specific upregulation, adenovirus with Sirt1 expression plasmids (Ad-Sirt1) or control vector (Ad-NC) was purchased from Genechem Co. (China). For Lcn2-specific downregulation, lentivirus with Lcn2-shRNA (sh-Lcn2#) (Target Sequence: #CGCTACTGGATCA-GAACATTT; ##GCCAGTTCCTCTGGGAAATA) or negative control (sh-NC) was structured by OBio Technology (China).

Full-length sequences for Sirt1, RelA/p65 and their various deletion mutants were cloned as previously described [21].

### 2.3. Cell viability assay

The mouse primary NP cells transfected with or without non-specific control or Ad-Sirt1 were cultured in 96-well multi-plates at  $5 \times 10^3$  cells/well, then IL-1β and EX-527 were administrated to specific wells. At the designated time points (0-, 24-, 48-, and 72-h), ten microliters of CCK reagent in a total volume of 100 μL were put into each well, before incubation for 4h. The absorbance at 450 nm was measured by an ELISA plate reader (SpectraMax i3, USA).

### 2.4. Immunofluorescence (IF)

The IF assay was conducted as previously described [22]. The appropriate Alexa Fluor 488-labeled or 647-labeled secondary antibodies were used at RT in dark, and the nucleus was dyed with DAPI (SouthernBiotech, USA). Images were acquired with Leica fluorescent microscope under the control of Leica LAS-X software.

### 2.5. RNA isolation and quantitative RT-PCR (qRT-PCR)

Total RNA of the above-mentioned cells was isolated by Trizol reagent (Invitrogen, USA) and reverse transcribed into cDNA using the HiScript III RT SuperMix for qPCR (Vazyme, China) following the manufacturer's description. Then, quantitative PCR was executed using ChamQ SYBR qPCR Master Mix (Vazyme, China) based on the Light-Cycler96 PCR system (Roche, Switzerland). All quantification of qPCR was normalized to GAPDH expression and performed by the comparative 2<sup>-ΔΔCT</sup> method. The designed primer sequences are listed in Supplement Table S1.

### 2.6. Construction of a single-cell cohort to compare normal and degenerative intervertebral discs

Three scRNA-seq datasets were integrated for a comprehensive analysis of cellular populations within human NP tissues. These datasets included GSE160756 with three normal NP samples of varying ages, GSE205535 with one normal and one degenerative NP sample, and GSE233666 with four degenerative NP samples. Data processing and analysis were conducted using the R package, allowing for accurate

clustering and characterization of diverse cell types in NP tissues.

### 2.7. Construction of bulk RNA sequencing libraries and sequencing

Total RNA was extracted from the samples by Trizol reagent separately. The RNA quality was checked by Agilent 2200 and kept at  $-80^{\circ}\text{C}$ . The RNA with RIN (RNA integrity number)  $> 7.0$  is acceptable for cDNA library construction. The cDNA libraries were constructed for each RNA sample using the TruSeq Stranded mRNA Library Prep Kit (Illumina, Inc.) according to the manufacturer's instructions. Generally, the protocol consists of the following steps: Poly-A containing mRNA was purified from 1  $\mu\text{g}$  total RNA using oligo (dT) magnetic beads and fragmented into 200–500 bp using divalent cations at  $94^{\circ}\text{C}$  for 5 min. The cleaved RNA fragments were used for first- and second-strand complementary DNA (cDNA) synthesis. The dUTP mix was used for second-strand cDNA synthesis, which allows for the removal of the second strand. The cDNA fragments were end repaired, A-tailed and ligated with indexed adapters. The ligated cDNA products were purified and treated with uracil DNA glycosylase to remove the second-strand cDNA. Purified first-strand cDNA was enriched by PCR to create the cDNA libraries. The libraries were quality controlled with Agilent 2200 and sequenced by HiSeq X (Illumina) on a 150 bp paired-end run. Bioinformatic analysis was performed using the OmicStudio tools at <https://www.omicstudio.cn/tool>.

### 2.8. Flow cytometry analysis

FITC Annexin V Apoptosis Detection Kits (Beyotime) was used and flow cytometry analysis [23] was performed according to the manufacturer's instructions.

### 2.9. Co-immunoprecipitation (Co-IP) and immunoblotting

Whole-cell lysates were extracted from mouse primary NP cells or HEK 293T cells. For immunoprecipitation (IP) assay, Pierce Crosslink Magnetic IP/Co-IP Kit (88805, Thermo, USA) was used according to the manufacturer's instructions. Immunoblotting was carried out as a previous study [24].

### 2.10. Luciferase reporter assay

To generate the Lcn2 promoter-activated luciferase reporter, -261bp to -252bp bp of Lcn2 promoter was cloned into PGL4.10 basic. Luciferase reporter assay was performed as previously described [24].

### 2.11. Chromatin immunoprecipitation (ChIP)-PCR

The ChIP assay was implemented using the ChIP kit (Millipore, USA) as previously described [25]. Briefly, primary mice NP cells were treated with or without 20 ng/mL IL-1 $\beta$  and respectively subjected to immunoprecipitation using either a control IgG or the ChIP-grade p65 (Proteintech, 10745-1-AP) after sonicated to an average fragment size of 300 bp. The co-precipitated chromatin was determined by PCR for the enrichment of promoter DNA using primers for Lcn2 (Forward: CCTGTTGCTCAACCTTGCCAC; Reverse: CCAAGTCCAGGAAGCCATGA).

### 2.12. Animals and IVDD model establishment

Animal use was approved by the Institutional Animal Care and Use Committee of Nanjing Medical University (approval number: IACUC-1709021), and Sirt1 transgenic (Sirt1<sup>TG</sup>) mice were generated in our laboratory previously [26].

Wild-Type C57BL/6 and Sirt1<sup>TG</sup> mice (4-week-old) were randomly divided into the Sham group or the IVDD group (6 mice per group). The skin of the caudal vertebra of mice in the Sham group was cut and sutured. Annulus fibrosus (AF) needle puncture of coccygeal discs was

used to build an IVDD model. After the mice were anesthetized, the operator sterilized the dorsal skin of the caudal spine with 75 % alcohol. Then a sterile scalpel was used to cut the skin on the surface of Co6-8 to locate the disc position for puncture. The incision of the Sham group was sutured subsequently. In the model group, an injection needle (26G) from a 1 mL syringe was used to pierce Co6/7, rotated  $180^{\circ}$ , and then held still for 10 s. All were postoperatively disinfected with 75 % alcohol at the suture.

### 2.13. Histopathology and immunohistochemistry (IHC)

The samples were fixed in 4 % PFA solution for 24h at RT, decalcified in EDTA-glycerol solution for 14–21 days, successively dehydrated, hyalinized, and embedded in paraffin, and sliced into 5- $\mu\text{m}$ -thick sections for histological staining including H&E and Safranin O staining or IHC as previously described [25]. The sections were observed by Leica fluorescent microscope. Histological Scores were calculated according to Boos classification [27].

### 2.14. Statistical analysis

All data expressed as the mean  $\pm$  standard deviation (SD) were analyzed and all graphs were presented by GraphPad Prism software (version 8.0, USA). To compare differences between groups, one-way ANOVA and student's t-test were used.  $p < 0.05$  was considered to indicate a statistically significant difference.

## 3. Results

### 3.1. Sirt1 was diminished in degenerated human intervertebral discs

To investigate cellular diversity, we constructed a single-cell cohort comprising normal and degenerative intervertebral discs, utilizing three single-cell RNA sequencing (scRNA-seq) datasets (three normal human NP tissues from GSE160756, one normal and one degenerative human NP tissue from GSE205535, and four degenerative human NP tissues from GSE233666). Following quality control and processing with Seurat, we obtained a total of 67,045 cells, of which 61,378 were annotated as NP cells (NPCs) (Fig. 1A). Using uniform manifold approximation and projection (UMAP) plots, hierarchical clustering, and gene expression signatures of published canonical markers, we annotated clusters into the following population partitions: nucleus pulposus cells (normal-NPCs, degenerative-NPCs, degenerative NP fibrocartilage, homeostatic chondrocytes, NP progenitor cells, proliferative-NPCs and MGP<sup>+</sup> NPCs), endotheliocytes, macrophages, and lymphocytes (Fig. 1B). The UMAP distribution of COL2A1 and SIRT1 gene expression in each cell type is displayed in the scatter plot (Fig. 1C and D), showing that SIRT1 was co-expressed with COL2A1 in cluster Normal-NPC. Compared to cluster Normal-NPC, the gene expression intensity of SIRT1 in Degenerative-NPC was lower (Fig. 1E). Furthermore, compared to normal-NPCs, the proportion of SIRT1<sup>+</sup> NPCs in IVDD NPCs was reduced (Fig. 1F). Gene ontology (GO) analysis revealed that SIRT1<sup>+</sup> NPCs were involved in protective biological processes, including cell cycle regulation, collagen biosynthesis, and connective tissue development (Fig. 1G).

To confirm the association between IVDD and Sirt1 expression, the NP tissue from patients was classified with Mild (G2-G4) or Severe (G5-G8) degeneration according to the modified Pfirrmann grading [20] by MRI (Fig. 1H). The mild degeneration group shows high T2 signal and normal disc height, while the severe group shows low T2 signal and reduced disc height. H&E staining manifested a disordered tissue structure with hypertrophic and vacuole-like cells in severe degeneration (Fig. 1I). Masson staining described the decreased ECM and disorganized collagen fibers alignment in samples with a high degree of degeneration (Fig. 1J). IHC staining uncovered that NP samples with severe degradation expressed significantly lower levels of Sirt1

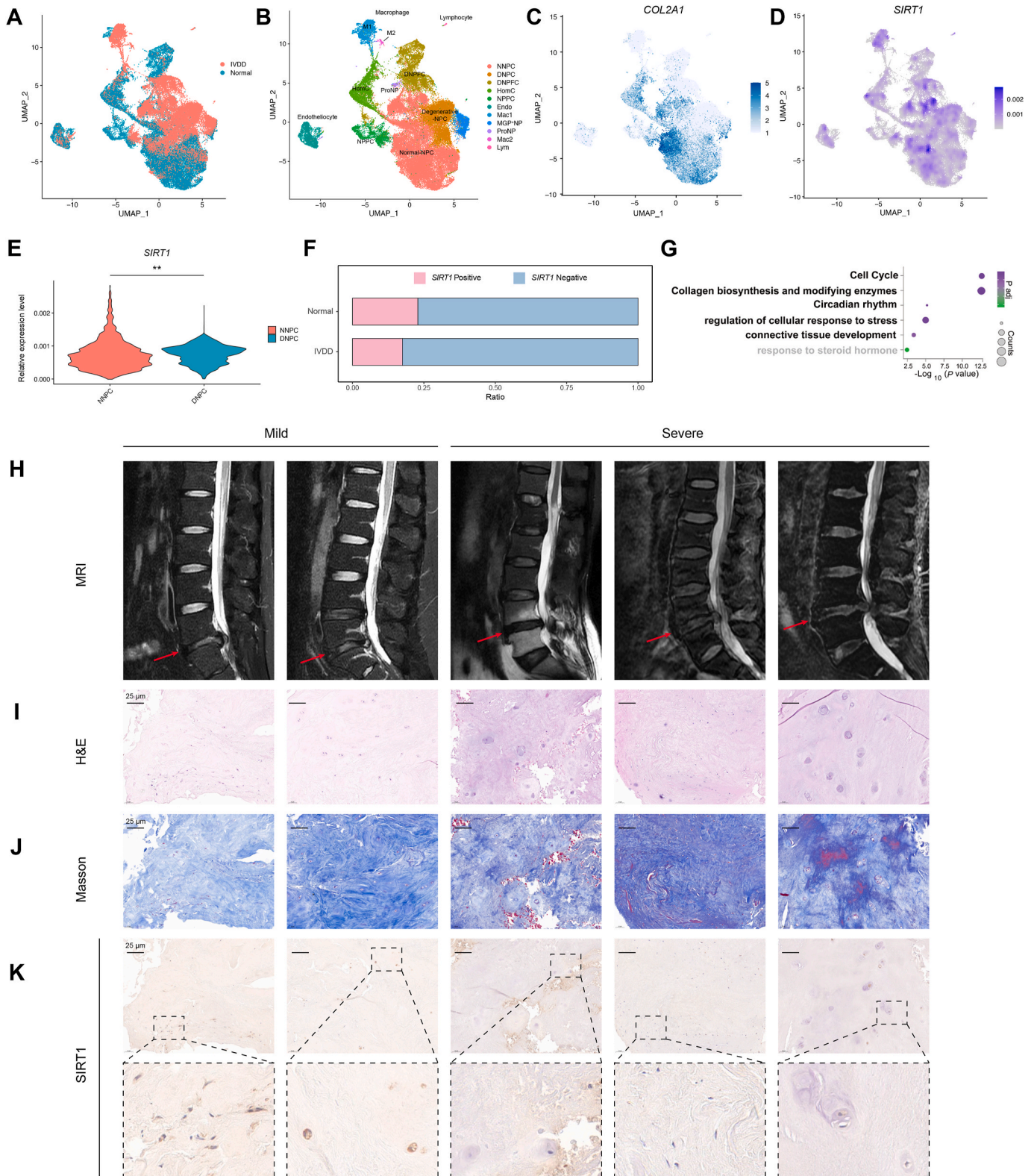


**Fig. 1.** Sirt1 expression was reduced in degenerative human NP specimens. (A) A combined UMAP showing all cells from normal and degenerative (IVDD) nucleus pulposus samples sourced from datasets GSE160756, GSE205535 and GSE233666. (B) UMAP map illustrating 11 distinct cell types: normal-NPCs (NNPC), degenerative-NPCs (DNPC), degenerative nucleus pulposus fibrocartilage (DNPFC), homeostatic chondrocytes (HomC), nucleus pulposus progenitor cells (NPPC), MGP<sup>+</sup> NPCs, endotheliocytes (Endo), macrophages (Mac, including M1 and M2 subtypes), proliferative NPCs (ProNP), lymphocytes (Lym). (C, D) UMAP images depicting *COL2A1* and *SIRT1* gene expression patterns. (E) Relative *SIRT1* expression levels in NNPC and DNPC clusters. (F) Bar plots representing the proportions of *SIRT1* positive (*SIRT1*<sup>+</sup>) NPCs and *SIRT1* negative (*SIRT1*<sup>-</sup>) NPCs. (G) Gene Ontology (GO) enrichment analysis of *SIRT1*<sup>+</sup> NPCs in biological processes. (H) Representative MRI images of human NP specimens from the Mild and Severe degeneration cases. Representative images of (I) H&E staining, (J) Masson staining, and (K) IHC staining of Sirt1 (scale bar: 25 μm) (Mild group: n = 10, Severe group: n = 10). \**p* < 0.05, \*\**p* < 0.01.

compared to those with mild degeneration (Fig. 1K).

These findings indicate that the Sirt1 expression was closely bound up with the degree of NP degeneration.

### 3.2. Sirt1 transgenic mice partially attenuated IVDD

To elucidate the role of Sirt1 in maintaining NP homeostasis *in vivo*, we generated Sirt1 transgenic C57BL/6 mice (Sirt1<sup>TG</sup>) (Supplement Figure A) [26]. Sirt1 mRNA and protein expression were observably higher in the intervertebral discs (IVDs) of 4-week-old Sirt1<sup>TG</sup> mice compared to wild-type (WT) littermates (Supplement Figure B, C).

Therefore, 4-week-old mice were selected for this study. Interestingly, Sirt1 expression in the IVDs was markedly lower in both 40-week-old WT and Sirt1<sup>TG</sup> mice compared to the 4-week-old counterparts, further supporting previous findings that Sirt1 expression was reduced in IVDD (Supplement Figure B, C).

We established a mouse IVDD model by puncturing the caudal vertebrae. MRI and X-Ray examination revealed that T2-weighted signals and disc height index (DHI) of Co6/7 IVDs in Sirt1<sup>TG</sup> mice were higher than those in WT mice with IVDD (Fig. 2A and B). As shown by H&E staining, Safranin O staining and histological scores, the annulus fibrosus (AF) of caudal discs in both Sirt1<sup>TG</sup> and WT sham groups were

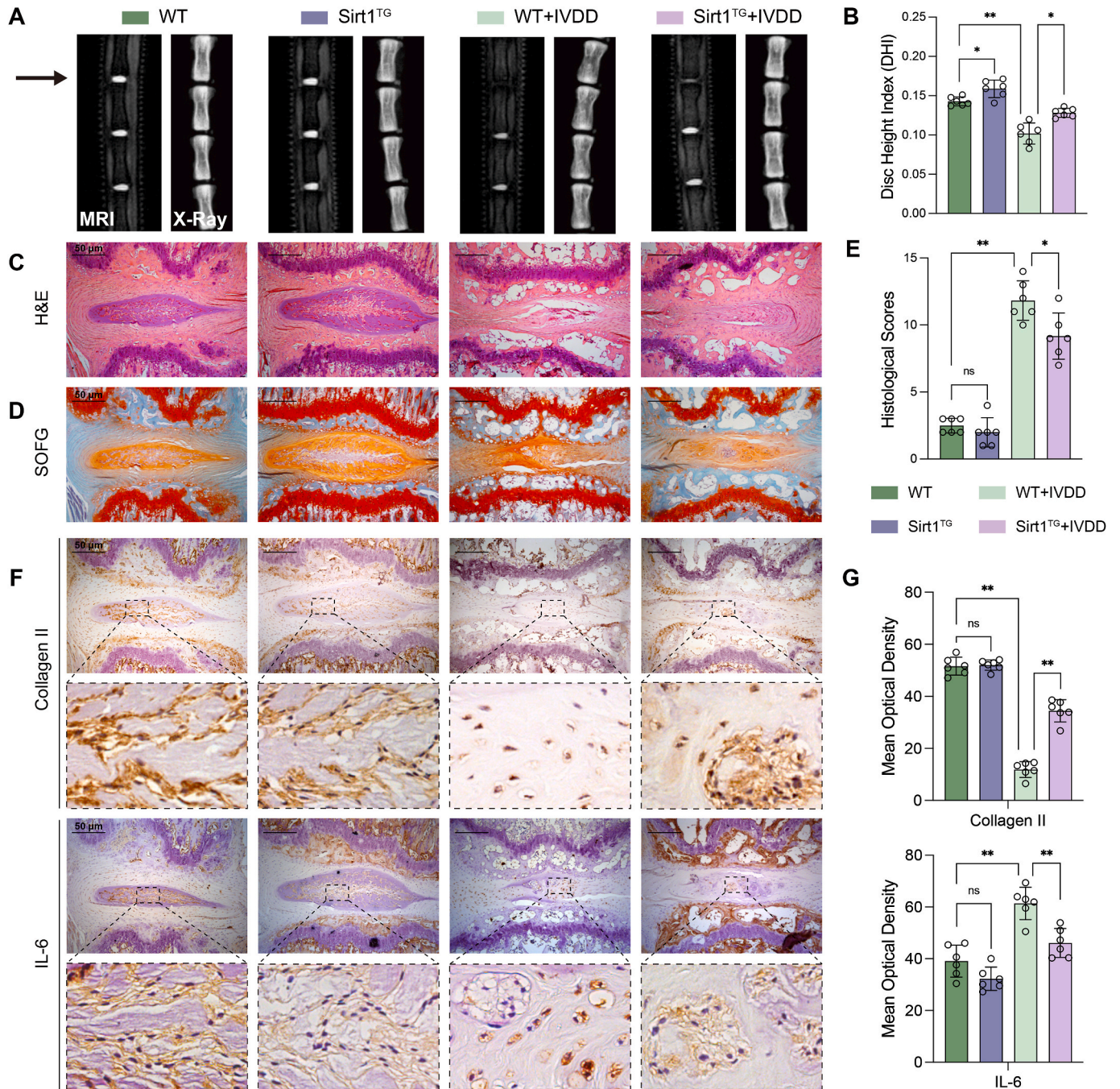


**Fig. 2.** Sirt1 transgenic mice delayed intervertebral disc degeneration. Representative images of (A) MRI and X-Ray, (C) H&E staining, (D) Safranin O-Fast Green staining, and (F) IHC staining in IVD specimens from Sirt1<sup>TG</sup> mice and their littermates, with or without caudal vertebrae puncture (scale bar: 50  $\mu$ m) (n = 6). (B) Intervertebral disc height index (DHI), (E) histological scores, and (G) quantitative analysis of Collagen II and IL-6 were measured in caudal vertebrae samples (n = 6). Data are presented as mean  $\pm$  SD, \**p* < 0.05, \*\**p* < 0.01.

well-organized, with enriched proteoglycan content in the NP and clear boundaries between NP and AF (Fig. 2C, D, E). Compared with the sham group, the caudal discs of WT puncture group showed localized cracks of AF, loss of NP cells in large volumes and replacement with vacuolar cells, leading to reduced disc height. In contrast, the Sirt1<sup>TG</sup> puncture group showed less damage, retained more concentric AF structures, and exhibited mostly scarred NP, which was beneficial for the maintenance of IVD height. IHC staining showed that high Collagen II expression in the NP of both WT and Sirt1<sup>TG</sup> sham groups (Fig. 2F and G). However, Collagen II levels were remarkably reduced in the IVDD groups due to NP replacement with fibrous tissue. Nevertheless, Sirt1<sup>TG</sup> mice exhibited

more abundant Collagen II in the NP compared to WT mice. In addition, IL-6 expression level, which indicated inflammatory response, was dramatically elevated in the NP of WT IVDD group compared to WT sham group. However, IL-6 was appreciably downregulated in the Sirt1<sup>TG</sup> IVDD group compared to WT IVDD group.

The above results demonstrate that Sirt1 overexpression in IVDs could postpone IVDD by suppressing inflammation in part.

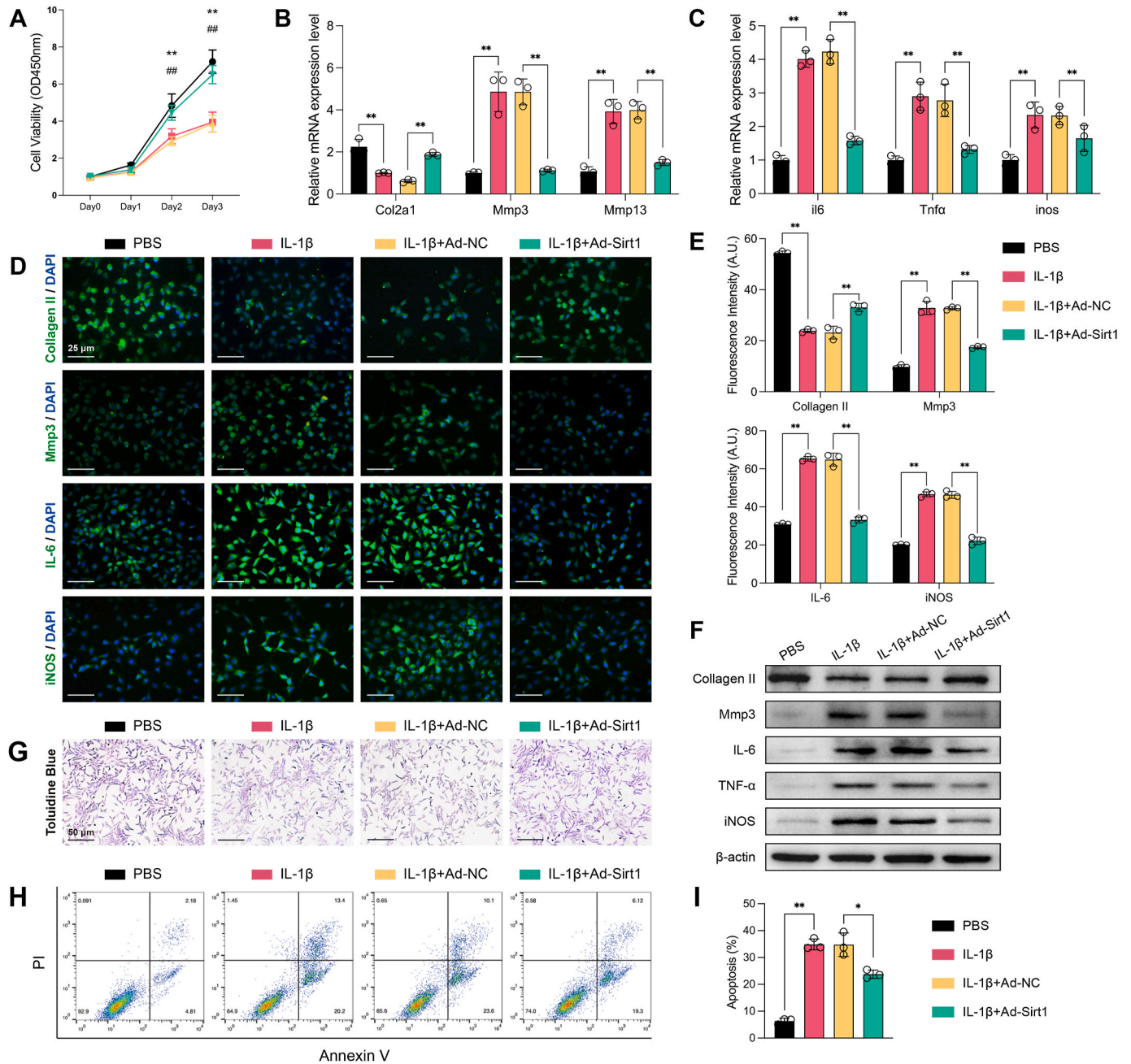


**Fig. 3.** Overexpression of Sirt1 inhibited ECM degradation and inflammatory response in NPCs. (A) Growth curves of NPCs under various treatments, assessed using the CCK-8 assay at 0, 24, 48, and 72 h (n = 3). \**p* < 0.05, \*\**p* < 0.01, comparing the IL-1 $\beta$ +Ad-Sirt1 group with the IL-1 $\beta$ +Ad-NC group; #*p* < 0.05, ##*p* < 0.01, comparing the IL-1 $\beta$  group with the PBS group. (B, C) qRT-PCR analysis of the mRNA expression of ECM-related indicators and inflammatory cytokines (n = 3). (D, E) Representative IF images and quantification of ECM-related indicators or inflammatory cytokines (scale bar: 25  $\mu$ m) (n = 3). (F) Western Blot analysis showing protein expression levels of ECM-related indicators or inflammatory cytokines (n = 3). (G) Representative images of Toluidine Blue staining across different groups. (scale bar: 50  $\mu$ m) (n = 3) (H, I) The apoptosis rate of NPCs, as assessed by flow cytometry (n = 3). Data are presented as mean  $\pm$  SD, \**p* < 0.05, \*\**p* < 0.01.

### 3.3. Sirt1 overexpression in NPCs prevented ECM degradation and inflammation induced by IL-1 $\beta$

To further verify whether Sirt1 overexpression could delay IVDD *in vitro*, we established an IL-1 $\beta$ -induced cell model. Mouse primary NPCs were infected with adenovirus (Ad-Sirt1 or Ad-NC) to create a Sirt1 overexpression model (Supplement Figure D, E). Cell Counting Kit-8 (CCK-8) assay demonstrated that NPCs proliferation activity significantly increased with higher Sirt1 expression compared to the IL-1 $\beta$ +Ad-NC group (Fig. 3A). We then examined the levels of ECM metabolism and inflammatory response in different NPCs using qRT-PCR, immunofluorescence, and Western Blot (Fig. 3B–F). Compared with the IL-1 $\beta$ +Ad-NC group, IL-1 $\beta$ +Ad-Sirt1 group showed a partial increase in Collagen II expression and a decrease in Mmp3 expression, suggesting that Sirt1 contributed to preserving ECM anabolism under IL-1 $\beta$  treatment. Similarly, the inflammatory markers IL-6, TNF- $\alpha$ , and iNOS were suppressed by Sirt1 overexpression. Toluidine Blue staining indicated that NPCs in the IL-1 $\beta$ +Ad-Sirt1 group exhibited more active ECM anabolism (Fig. 3G). Additionally, we analyzed the degree of apoptosis in different NPCs using flow cytometry (Fig. 3H and I). The results showed that fewer NPCs in the IL-1 $\beta$ +Ad-Sirt1 group experienced apoptosis in comparison with the IL-1 $\beta$ +Ad-NC group.

These findings indicate that Sirt1 overexpression could partially alleviate the degree of NPCs degeneration by inhibiting ECM degradation and inflammatory response.

### 3.4. Sirt1-driven modulation of ECM homeostasis and inflammation in NPCs through NF- $\kappa$ B pathway suppression

To delve into the functions of Sirt1 and the potential molecular mechanisms underlying its inhibition of the inflammatory response in primary NPCs, we conducted further research using bulk RNA sequencing (RNA-seq). Differentially expressed genes (DEGs) were first analyzed between Ad-NC and Ad-Sirt1 NPCs both after IL-1 $\beta$  stimulation, with each group containing three biological replicates. A total of 1,350 significantly up-regulated genes and 324 significantly down-regulated genes were filtered according to  $\log_2FC > 1$  or  $< -1$  and  $FDR < 0.05$  (Fig. 4A). Consistent with the earlier findings, NPCs transfected Ad-Sirt1 exhibited considerable restraint of ECM catabolism, including regulation of genes such as *Col2a1*, *Mmp3*, and *Sox9* (Fig. 4B). Importantly, the expression of various cytokines and chemokines associated with inflammation was inversely related to Sirt1 expression (Fig. 4B). Kyoto Encyclopedia of Genes and Genomes (KEGG) analysis and Gene set enrichment analysis (GSEA) revealed that Sirt1 overexpression was positively correlated with ECM receptor interaction and focal adhesion (Fig. 4C). GO analysis showed that down-regulated DEGs in the biological process category were correlated with inflammatory response and NF- $\kappa$ B regulation (Fig. 4D). These results imply that Sirt1 modulates inflammatory response and ECM synthesis in NPCs, highlighting the importance of the NF- $\kappa$ B pathway.

Aiming to determine the truth of the above conjecture, we used Western Blot and IF to show that IL-1 $\beta$  significantly boosted the p-p65/p65 ratio and enhanced the nuclear translocation of p65 compared to the control group. However, the IL-1 $\beta$ +Ad-Sirt1 group partially mitigated these effects compared to the IL-1 $\beta$ +Ad-NC group. Moreover, inhibition of Sirt1 activity in the IL-1 $\beta$ +Ex527 group further activated NF- $\kappa$ B compared to the IL-1 $\beta$  group (Fig. 4E and F). Then, our investigation used Bay11-7082, a specific inhibitor of the NF- $\kappa$ B signaling pathway, to reveal that the p-p65 and Mmp3 expression were down-modulated in the IL-1 $\beta$ +Ex527+Bay11-7082 group compared to the IL-1 $\beta$ +Ex527 group, while Collagen II expression were unmodulated; simultaneously, the inflammatory factors IL-6, iNOS, and TNF- $\alpha$  were markedly decreased (Fig. 4G and H).

These results show that inhibition of the NF- $\kappa$ B is a crucial mechanism by which Sirt1 regulates inflammation.

### 3.5. Sirt1 suppressed NPCs degradation by promoting the deacetylation of the RelA/p65 subunit

Deacetylation of RelA/p65 has been reported as a crucial mechanism for inhibiting its phosphorylation. Next we measured the relationship between Sirt1 expression and the acetylation or phosphorylation of p65 in NPCs using Co-IP (Fig. 5A). As anticipated, overexpression of Sirt1 significantly reduced the acetylation of p65 at the K310 site and inhibited p65 phosphorylation at Ser536 compared to the negative control group. Subsequently, we investigated which domains of Sirt1 and p65 are responsible for their interaction. We employed Flag-labeled Sirt1 fragments and HA-labeled p65 fragments to identify the binding region in HEK 293T cells or NPCs (Fig. 5B). Consequently, deletion of the N-terminus ( $\Delta$ N) did not affect the interaction between Sirt1 and p65, whereas deletion of C-terminus abolished their combination (Fig. 5C and E). The human RelA/p65 shares the conserved Rel homology domain (RHD) with the Rel/NF- $\kappa$ B family and a nuclear localization signal (NLS) at the C-terminal end of RHD [28]. Additionally, there are three transcriptional activation domain (TA1/2/3) at the C-terminus of p65 (Fig. 5B). The study revealed that the RHD-NLS domain of p65 was responsible for its interaction with Sirt1 (Fig. 5D and F).

This shows that Sirt1 could impair the Ser536 phosphorylation and suppress nuclear translocation of the RelA/p65 by enhancing K310 deacetylation, thereby elucidating the underlying mechanism of their interaction.

### 3.6. Lipocalin 2 acted as a key target of Sirt1-mediated NF- $\kappa$ B suppression *in vitro*

According to the *p*-values and potential biological functions of DEGs in RNA-seq, we selected *Saa3*, *Lcn2*, and *Timp3* for further investigation (Fig. 6A). To ascertain whether *Saa3*, *Lcn2*, and *Timp3* were regulated by the NF- $\kappa$ B signaling pathway, NPCs were treated with different concentrations of its specific inhibitor Bay11-7082. The qRT-PCR data revealed that *Saa3* and *Lcn2* were dramatically downregulated

after 2 h of co-stimulation of NPCs with IL-1 $\beta$  and 1.0  $\mu$ M Bay11-7082 compared to IL-1 $\beta$  treatment alone, while *Timp3* expression remained unaffected (Fig. 6B). In contrast to the IL-1 $\beta$  group, mRNA expression of *Saa3* and *Lcn2* was significantly decreased in the IL-1 $\beta$ +Ad-Sirt1 group and further dropped with the increase in the multiplicity of infection (MOI), whereas *Timp3* mRNA expression visibly rebounded after Sirt1 overexpression (Fig. 6B). Compared to the IL-1 $\beta$  group, *Saa3* and *Lcn2* were further upregulated after inhibiting Sirt1 (IL-1 $\beta$ +Ex527), while *Timp3* expression did not change significantly, indicating a clear negative correlation between the expression of *Saa3* and *Lcn2* with Sirt1 expression (Fig. 6B). Next, Western Blot and IF showed that, compared to the IL-1 $\beta$  group, *Lcn2* expression was notably reduced in NPCs from the IL-1 $\beta$ +Ad-Sirt1 group and the IL-1 $\beta$ +Bay11-7082 group, suggesting an association between *Lcn2* and the Sirt1 and NF- $\kappa$ B signaling pathways (Fig. 6C and D). The UMAP distribution of *LCN2* expression revealed that *LCN2* was enriched in the Degenerative-NPC cluster (Fig. 6E and F). Based on UMAP and hierarchical clustering, four subtypes of Degenerative-NPCs were further identified, as shown in Fig. 6G. The Sub-cluster 1 was particularly enriched with Degenerative-NPCs exhibiting high *LCN2* expression (Fig. 6H). Thus, *Lcn2* could be downstream of NF- $\kappa$ B dysregulation mediated by Sirt1, leading to IVDD progression.

To further elucidate the connection between *Lcn2* and the NF- $\kappa$ B signaling pathway, we used the JASPAR database to predict the binding sites of RelA/p65 and the human *LCN2* (*hLCN2*) promoter region. Through bioinformatics analysis, we identified a common putative binding site "gggaatgtcc" for RelA/p65 within the promoter region of *hLCN2* and mouse *Lcn2* (*mLcn2*) (Fig. 6I and J). To validate the influence of inflammation on p65-regulated *Lcn2* transcriptional activity, we designed primers at 300 bp containing the aforementioned predicted site and analyzed IL-1 $\beta$ - or PBS-treated NPCs by ChIP-PCR, revealing

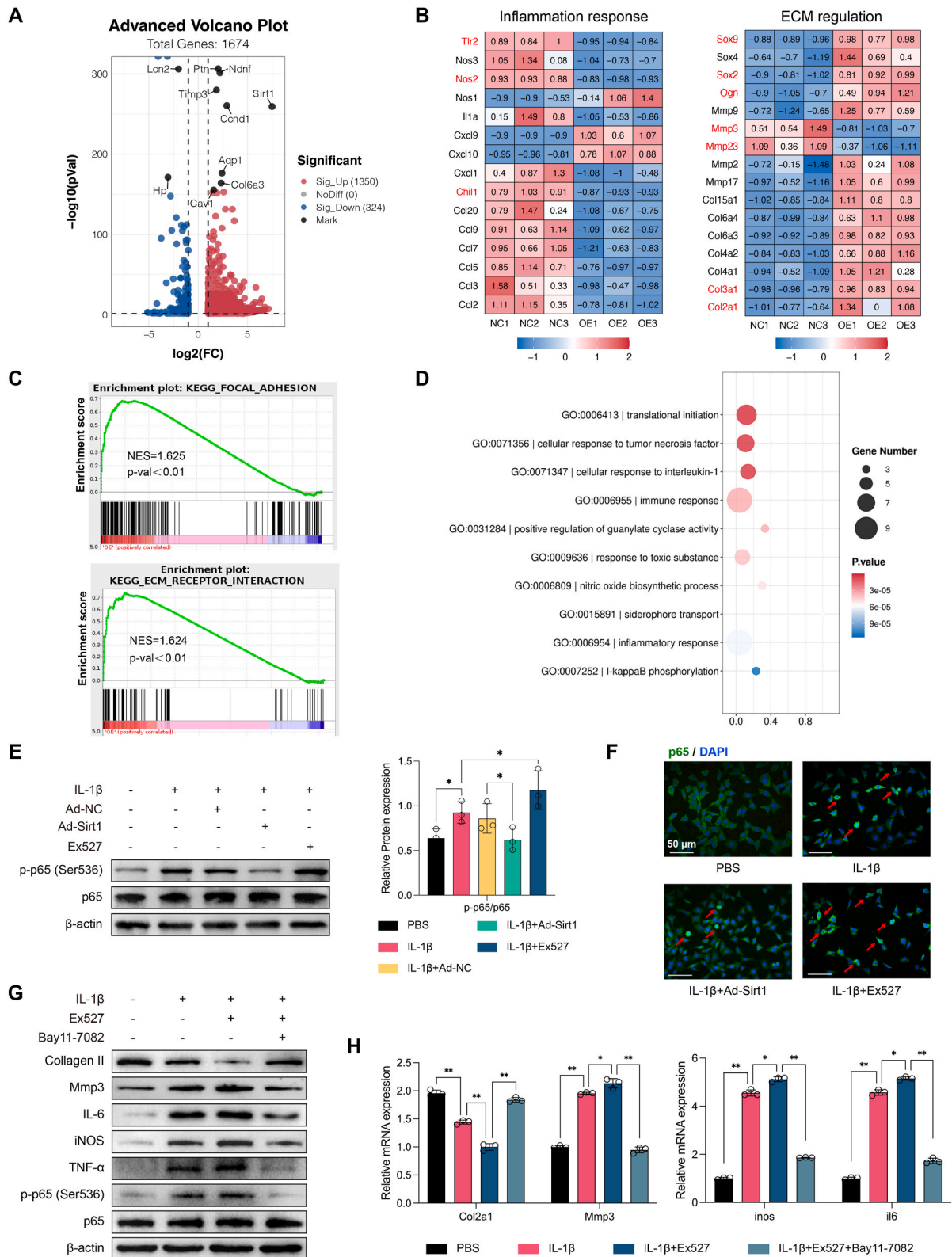


**Fig. 4.** RNA-seq and bioinformatics analysis revealed that Sirt1 suppresses NF-κB signaling pathway in NPCs. (A) Volcano plot highlighting significant DEGs between the IL-1β+Ad-NC and IL-1β+Ad-Sirt1 groups. (B) Heatmaps (Log<sub>2</sub> fold change) showing significant changes (p < 0.05) in inflammatory cytokines and ECM organization-related genes in the Sirt1 overexpression group versus the negative control. (C) KEGG and GSEA analysis were performed to interpret the DEGs distribution related to ECM metabolism regulation. (D) Top 10 GO enrichment terms for downregulated DEGs in biological processes. (E) Western Blot analysis and quantitation of p65 and p-p65 protein expression in NPCs under different treatments (n = 3). (F) Representative IF images of p65 in NPCs under different treatments (scale bar: 50 μm) (n = 3). (G) Western Blot analysis of protein expression and (H) qRT-PCR analysis of mRNA expression in NPCs under different treatments (n = 3). Data are presented as mean ± SD, \*p < 0.05, \*\*p < 0.01.



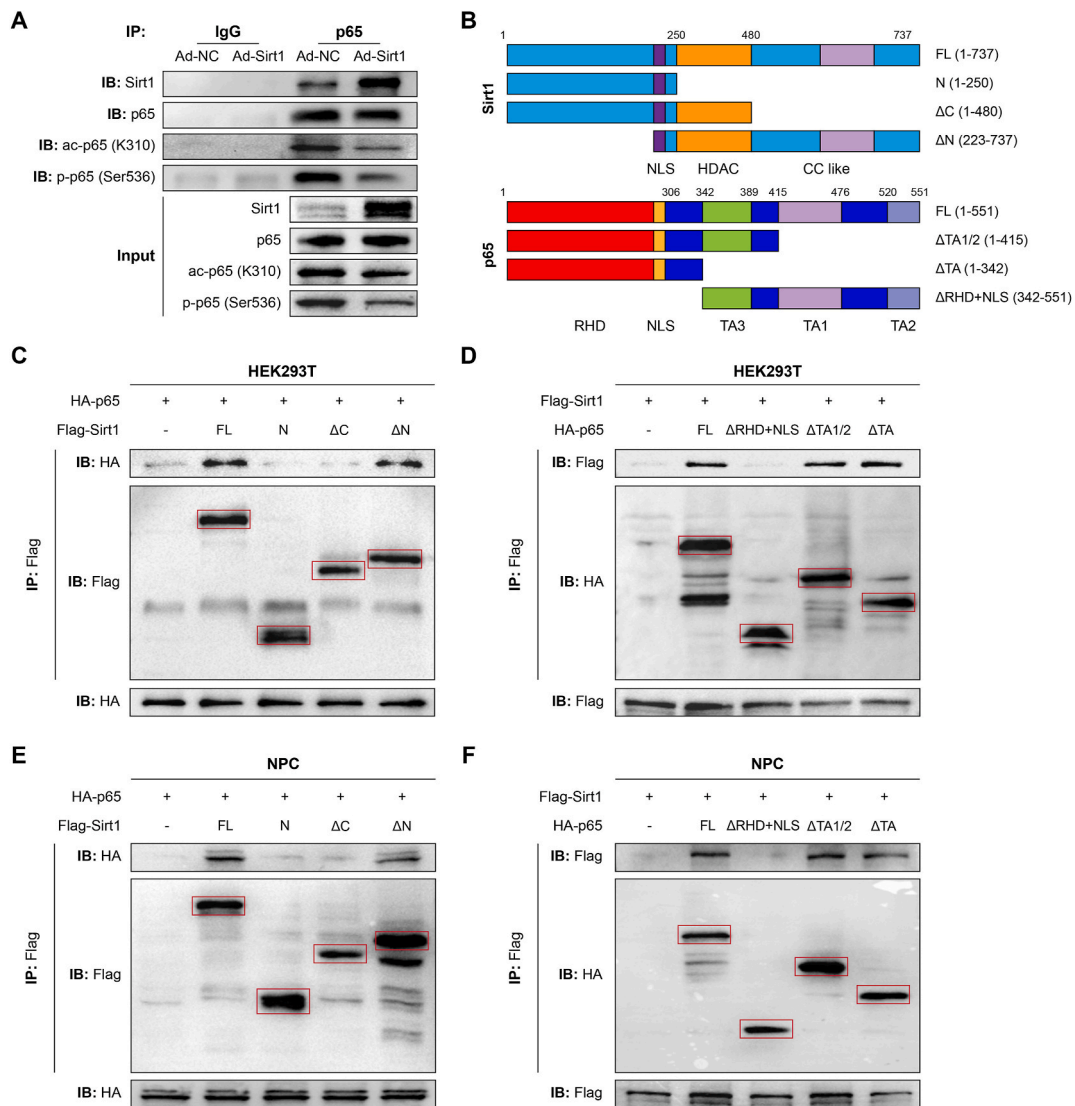


**Fig. 5.** Sirt1 interacted with RelA/p65 and deacetylated it in NPCs. (A) Co-IP and Western Blot analysis of acetylation and phosphorylation levels of p65 protein in NPCs transfected with Ad-NC or Ad-Sirt1 ( $n = 3$ ). (B) Schematic diagrams of Flag-tagged Sirt1 full-length (FL), HA-tagged p65 FL and their various deletion mutants. (C, E) HEK 293T cells and NPCs were co-transfected with HA-p65 FL and Flag-tagged Sirt1 FL or its deletion mutants or vectors. Co-IP and Western Blot detected whole-cell lysates using anti-HA and anti-Flag ( $n = 3$ ). (D, F) HEK 293T cells and NPCs were co-transfected with Flag-tagged Sirt1 FL and HA-p65 FL or their deletion mutants or vectors. Co-IP and Western Blot detected whole-cell lysates using anti-HA and anti-Flag ( $n = 3$ ).

that the inflammatory response notably enhanced the binding of p65 to the *mLcn2* promoter (Fig. 6K). The *Lcn2* promoter mutant plasmid (MUT) was constructed through deletion mutation (Fig. 6L). The luciferase reporter showed that p65 was able to bind to the predicted site in the *mLcn2* promoter region, and the deficiency of the critical binding site resulted in a strikingly lower binding ability, suggesting that p65 has at least one binding site with the *Lcn2* promoter region (Fig. 6M).

These findings indicate that p65 could interact with the *Lcn2* promoter region when inflammation occurs, thereby substantially promoting the transcription of *Lcn2*.

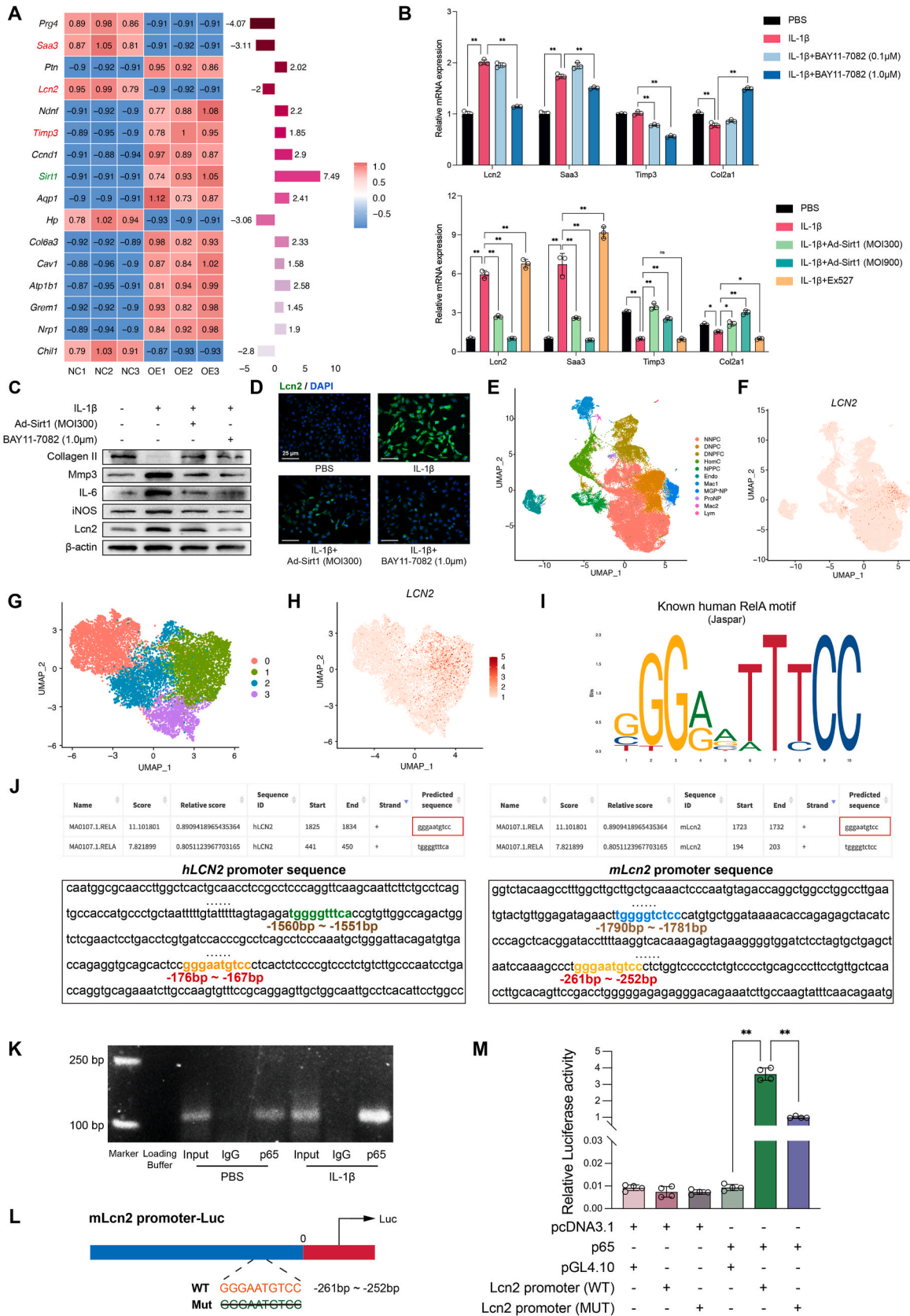
### 3.7. Lipocalin 2 was a latent molecule that recruited macrophages and promoted M1 polarization to aggravate inflammation

According to the single-cell cohort derived from three scRNA-seq datasets, we noticed that the proportion of macrophages in IVDD NP tissue was higher compared to normal control samples, particularly M1-like macrophages (Fig. 7A). Correlation analysis revealed a positive association between the proportion of *LCN2*<sup>+</sup> Degenerative-NPCs and

*IL1B*<sup>+</sup> macrophages (Fig. 7B), suggesting that macrophage (M $\phi$ ) infiltration played a key role in the inflammatory microenvironment of IVDD, and *LCN2* derived from Degenerative-NPCs may act as a cytokine that regulates macrophages.

To unravel the role of *Lcn2* in mouse primary NPCs, our study utilized a lentivirus to deliver two different shRNAs to knock down the endogenous *Lcn2* expression (Supplement Figure F, G). Then we established a co-culture system to elucidate the role of *Lcn2* in M $\phi$  (Fig. 7C). Transwell assay indicated that Raw264.7 cells co-cultured with sh-*Lcn2* NPCs displayed lower migratory ability than those co-cultured with sh-NC NPCs after IL-1 $\beta$  treatment (Fig. 7D and E). Raw264.7 cells expressed high levels of M1-relevant cytokines (iNOS and IL-6) when co-cultured with NPCs under IL-1 $\beta$  stimulation compared to the PBS control. However, this result was altered by co-culture with sh-*Lcn2* NPCs (Fig. 7F and G). Next, we stimulated Raw264.7 cells with recombinant mouse *Lcn2* (rm*Lcn2*), and found that *Lcn2* promoted M $\phi$  migratory ability and M1-markers expression in a dose-dependent manner (Fig. 7H–K).

These measurements confirm that *Lcn2* promotes M $\phi$  recruitment and M1 polarization, thus exacerbating the chronic inflammatory



(caption on next page)

**Fig. 6.** *Lcn2* was a critical target of the Sirt1/NF- $\kappa$ B axis. (A) Heatmap with bar plot (Log<sub>2</sub> fold change) showing the top 16 most statistically significant DEGs from mRNA-seq. (B) qRT-PCR analysis of mRNA expression levels of *Lcn2*, *Saa3*, and *Timp3* in NPCs with NF- $\kappa$ B suppression, or with Sirt1 overexpression or activity inhibition (n = 3). (C) Western Blot analysis of protein expression levels in NPCs under different treatments (n = 3). (D) Representative IF images and quantitative analysis of *Lcn2* in NPCs under different treatments (scale bar: 25  $\mu$ m) (n = 3). (E) UMAP map of the 11 cell types identified in the scRNA-seq datasets. (F) UMAP image showing *LCN2* gene expression. (G) UMAP plot of degenerative NPCs (DNPC), profiling four sub-clusters and (H) UMAP image showing *LCN2* expression across these sub-clusters. (I) Sequence logo representing the binding specificity of human RelA/p65, sourced from the JASPAR database. (J) Predicted RelA/p65 binding sites in the human and mouse *Lcn2* promoter region. (K) Representative image of ChIP-PCR showing the *Lcn2* promoter fragment using anti-p65 in NPCs with or without IL-1 $\beta$  (n = 3). (L) Schematic diagram of WT or Mutant plasmid of the mouse *Lcn2* promoter region. (M) Dual-luciferase activity of HEK 293T cells co-transfected with p65 or a pcDNA3.1 vector and the *Lcn2* promoter (WT) or its deletion mutant and a pGL4.10 vector (n = 4). Data are presented as mean  $\pm$  SD, \**p* < 0.05, \*\**p* < 0.01.

microenvironment in IVDs.

#### 4. Discussion

Intervertebral discs (IVDs) are able to withstand mechanical stress and maintain flexibility due to the proteoglycan-rich nucleus pulposus (NP) and the tightly arranged layers of the annulus fibrosus (AF). The primary nutrient supply for both the NP and AF comes from the cartilaginous endplates (CEP) [29]. Further investigations suggests that intervertebral disc degeneration (IVDD), as age-related pathophysiological process, results from a combination of factors such as prolonged pressure stimulation [30], aging [13], oxidative stress [31], autophagy [8], and an acute or chronic inflammatory microenvironment [32,33]. Together, these factors lead to a decrease in cell numbers and significant extracellular matrix (ECM) degradation.

*Sirt1*, a well-known longevity-associated gene, has garnered widely attention and been extensively studied. Prior studies demonstrated its role in promoting bone formation and enhancing nucleus pulposus cell (NPC) function by stimulating cell proliferation and proteoglycan synthesis [26,34]. Despite earlier studies have documented a marked reduction in Sirt1 protein expression levels in IVDs [15,35], the relationship between Sirt1 expression and the progression of IVDD across different degeneration stages had not been fully established. In this study, we integrated MRI and histopathological staining to categorize disc degeneration and observed a clear reduction in Sirt1 expression as degeneration severity increased. Furthermore, single-cell RNA sequencing (scRNA-seq) analysis was used to identify cellular diversity within both normal and degenerated discs, showing a marked decrease in *SIRT1* expression within degenerative NPCs compared to normal ones. Gene ontology (GO) analysis indicated that *SIRT1*<sup>+</sup> NPCs are involved in key biological processes. The loss of Sirt1, therefore, may disrupt these protective mechanisms and accelerate IVDD progression. These findings suggest that Sirt1 deficiency is not only a marker of disc degeneration but may also contribute directly to the pathological changes observed in IVDD by impairing critical cellular functions. As a result, Sirt1 represents a promising therapeutic target for slowing or preventing further degeneration in patients with IVDD, highlighting the potential of Sirt1-based therapies in maintaining intervertebral disc homeostasis and function.

The inflammatory cascade response is recognized as a critical factor in the acute exacerbation of low back pain associated with IVDD [36]. During IVDD progression, there is a substantial release of pro-inflammatory cytokines, including IL-1 $\beta$ , IL-6, TNF- $\alpha$ , as well as various chemokines [37]. In our work, we developed an *in vitro* inflammation model by treating primary mouse NPCs with IL-1 $\beta$  and overexpressing Sirt1 via adenovirus. Our findings demonstrated that Sirt1's protective role by promoting ECM anabolism and mitigating the impact of inflammatory stimuli. *In vivo*, we utilized Sirt1 transgenic C57BL/6 mice (Sirt1<sup>TG</sup>) to further investigate Sirt1's role in IVDD [26]. Sirt1 protein and mRNA expression in the IVDs tissue of 4-week-old Sirt1<sup>TG</sup> mice were significantly elevated compared to wild-type (WT) mice, confirming the successful overexpression of Sirt1. However, both 40-week-old Sirt1<sup>TG</sup> mice and WT mice exhibited reduced Sirt1 expression, indicating that Sirt1 levels decline with age in the IVD, a trend consistent with findings in other tissues, including the spleen,

testis, and thymus [38]. Notably, our previous work established a mouse model of IVDD using tail suspension to induce IVD stress, resulting in significant disc senescence [13,25]. In the present study, we focused on the inflammatory response in IVDD using a needle-puncture model, which strongly simulates inflammation [14]. Histological analyses, including H&E, Safranin O-Fast Green, and IHC staining, demonstrated that Sirt1<sup>TG</sup> mice exhibited lower levels of inflammation and enhanced ECM synthesis, thereby alleviating the degenerative process. These results suggest that Sirt1 plays a pivotal role in maintaining disc homeostasis by modulating inflammatory responses and promoting ECM anabolism.

As mentioned previously, chronic inflammatory responses, characterized by the continuous release of pro-inflammatory cytokines, disrupt ECM metabolism and activate several inflammation-related signaling pathways, including the TLR signaling pathway, p38 MAPK pathway [32], JAK/STAT signaling pathway [39], and NF- $\kappa$ B signaling pathway [40], perpetuating an unrelenting of the inflammatory microenvironment. In the study, we used bulk RNA sequencing to compare DEGs in NPCs with and without Sirt1 overexpression under IL-1 $\beta$  stimulation, identifying a potential regulatory role for Sirt1 in the NF- $\kappa$ B signaling pathway. Our results demonstrated that Sirt1 overexpression effectively suppressed IL-1 $\beta$ -induced activation of the NF- $\kappa$ B signaling pathway, highlighting Sirt1's anti-inflammatory function. Specifically, p65 phosphorylation levels were significantly elevated upon Sirt1 inhibition, aligning with previous studies [14,41]. Moreover, by utilizing the specific NF- $\kappa$ B inhibitor Bay11-7082, we confirmed that NF- $\kappa$ B inhibition is a crucial mechanism through which Sirt1 modulates the inflammatory response. These findings underscore the critical role of Sirt1 in maintaining intervertebral disc homeostasis, particularly in mitigating chronic inflammation and preventing degenerative changes associated with IVDD.

Post-Translational Modification (PTM) is an important modality for regulating protein activity, with acetylation being one of the most widespread PTMs involved in transcription, DNA damage repair, cell division, and signal transduction [42]. Proteins often undergo multiple PTMs, which can influence one another. For instance, acetylation has been shown to modulate phosphorylation, methylation, and ubiquitination, thereby dynamically regulating cellular signaling processes [42, 43]. Previous studies have reported that the histone acetyltransferase cAMP-response element-binding protein-binding protein (CBP) acetylates Foxo1, facilitating its phosphorylation at Ser-253 by PKB [44]. In our study, we utilized Co-IP assay to demonstrate that p65 physically interacts with Sirt1 in primary NPCs, and both p65 K310 acetylation and Ser536 phosphorylation were suppressed by Sirt1. Previous reports have shown that the N-terminal Rel homology domain of p65 physically interacts with other protein, such as PPAR $\delta$  and COMMD10 [45,46]. Here, our study further demonstrated that RelA/p65 binds to the C-terminus of Sirt1 through the RHD-NLS domain (p65<sup>1-342</sup>), thus explaining that lysine 310 acetylation of p65 may be a key underlying factor in activating the transcription of target gene.

Currently, few studies have reported on specific downstream molecules transcriptionally regulated by Sirt1 through inhibition of the NF- $\kappa$ B pathway. In this study, we identified *Saa3*, *Lcn2*, and *Timp3* as potential downstream targets through RNA-seq analysis. Among these, *Lcn2* demonstrated a significant negative correlation with NF- $\kappa$ B

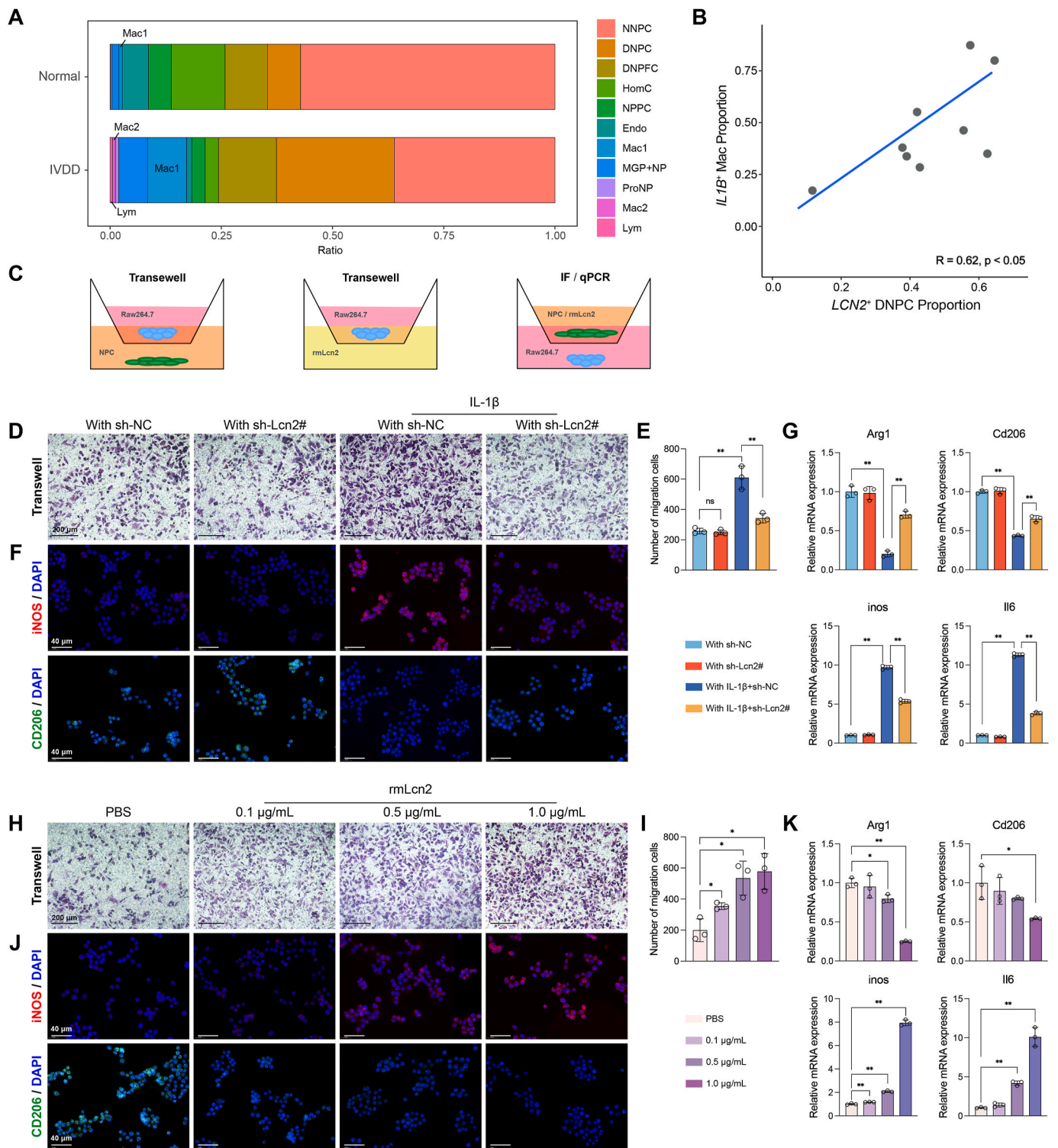


**Fig. 7.** Lcn2 exerts an influence on recruitment of M $\phi$  and M1 polarization. (A) Bar plots representing the proportion of above-mentioned 11 cell types identified in normal and IVDD NP tissue based on scRNA-seq datasets. (B) Correlation analysis between the proportion of *LCN2*<sup>+</sup> DNPCs and *IL1 $\beta$*  + Macrophages. (C) Schematic diagrams of the co-culture system. Raw264.7 cells were cultured in the upper chamber, while NPCs or F12/DMEM with varying concentrations of rmLcn2 were seeded or added in the lower chamber of the Transwell assay. The aforementioned cells were cultured in reverse position for IF and qRT-PCR. (D, E) Representative Transwell images and quantification of Raw264.7 cells co-cultured with sh-NC or sh-Lcn2 NPCs, with or without IL-1 $\beta$  (scale bar: 200  $\mu\text{m}$ ) (n = 3). (F) Representative IF images showing the expression of M $\phi$  markers in Raw264.7 cells co-cultured with sh-NC or sh-Lcn2 NPCs, with or without IL-1 $\beta$  (scale bar: 40  $\mu\text{m}$ ) (n = 3). (G) qRT-PCR analysis of mRNA expression of M $\phi$  markers in Raw264.7 cells co-cultured with sh-NC or sh-Lcn2 NPCs, with or without IL-1 $\beta$  (n = 3). (H–I) Representative Transwell images and quantification of Raw264.7 cells treated with different concentrations of rmLcn2 (scale bar: 200  $\mu\text{m}$ ) (n = 3). (J) Representative IF images of the expression of M $\phi$  markers in Raw264.7 cells treated with different concentrations of rmLcn2 (scale bar: 40  $\mu\text{m}$ ) (n = 3). (K) qRT-PCR analysis of mRNA expression of M $\phi$  markers in Raw264.7 cells treated with different concentrations of rmLcn2 (n = 3). Data are presented as mean  $\pm$  SD, \* $p$  < 0.05, \*\* $p$  < 0.01.

signaling and Sirt1 expression. The UMAP analysis revealed that *LCN2* was highly expressed in a specific subtype of Degenerative-NPCs. *Lcn2*, a lipocalin predominantly found in neutrophils, is known to covalently bind to matrix metalloproteinase 9 (MMP9) [18]. Recent research has highlighted its role in maintaining cartilage homeostasis and growth plate development [47]. However, no study has reported on the involvement of *Lcn2* in IVDD. Using luciferase reporter assay, we demonstrated that RelA/p65 acts as a transcriptional regulator of *Lcn2*. Furthermore, ChIP-PCR analysis revealed that the IL-1 $\beta$ -induced inflammatory response significantly enhanced the binding of RelA/p65 to *Lcn2* promoter regions. Our research uncovered, for the first time, *Lcn2* as a crucial downstream effector in Sirt1-mediated regulation of NF- $\kappa$ B activity.

*Lcn2*, primarily expressed by neutrophils, has been linked to the infiltration of inflammatory cells such as neutrophils and macrophages (M $\phi$ ) in conditions like non-alcoholic steatohepatitis [48]. Recent studies have shown an increased presence of M $\phi$  within AF, NP and CEP regions, particularly in higher grades of disc degeneration [49,50]. Analysis of single-cell RNA sequencing data revealed an increased proportion of macrophages, particularly M1-like macrophages, in IVDD NP tissue compared to normal NP tissue. Correlation analysis suggests that *LCN2* derived from Degenerative-NPCs may regulate macrophage infiltration and contribute to the inflammatory microenvironment in IVDD. In our study, we employed a co-culture system to investigate whether *Lcn2* plays a role in M $\phi$  activity in IVDD. Transwell assay confirmed that *Lcn2* promotes M $\phi$  recruitment, while IF and qRT-PCR assays demonstrated that *Lcn2* induces M1 polarization, thereby exacerbating the chronic inflammatory microenvironment during IVDD. These findings align with previous research by Wang et al., who observed that the production of IL-6, IL-1 $\beta$ , TNF- $\alpha$ , and iNOS was suppressed in *Lcn2*<sup>-/-</sup> M $\phi$  [51]. However, our study reveals that *Lcn2* derived from NPCs, rather than from macrophages, plays a crucial role in fostering the inflammatory microenvironment and serves as a key initiator in the vicious cycle of IVDD.

In summary, our present findings reveal that dysfunction of the Sirt1/NF- $\kappa$ B/*Lcn2* axis exerted an influence on macrophages recruitment and M1 polarization, subsequently exacerbating the chronic inflammatory microenvironment during IVDD (Fig. 8), offering new perspectives for future cellular and molecular therapies targeting this axis for low back pain.

## Authors' Contributions

YFW: Conceptualization, Methodology, Investigation, Writing – original draft. HLZ, LZL, and YL: Methodology, Investigation, Formal analysis. HL, ZL, FLY, TJ and TYZ: Methodology, Investigation. FX and CM: Supervision, Conceptualization, Methodology, Writing – original draft, and finalizing of the study. YXR: Project administration, Conceptualization, Supervision, Methodology, Writing – original draft, and finalizing of the study.

## Ethics approval and consent to participate

Human subjects: This work was implemented with the approval of the Ethics Committee of the First Affiliated Hospital of Nanjing Medical University (approval number: 2018 SR-233). Prior to the operation, informed consent was obtained from all patients, including their voluntary donation of the diseased nucleus pulposus tissue extracted during the operation, and their consent for all specimens to be used for scientific research and for the results obtained to be published in scientific journals. Animal experimentation: Animal use was approved by the Institutional Animal Care and Use Committee of Nanjing Medical University (approval number: IACUC-1709021).

## Data availability statement

The datasets used and/or analyzed during the current study are available from the corresponding author on reasonable request.

## Funding statement

This study was financially supported by the National Natural Science Foundation of China (81572149 and 82372483), Sino-German Mobility program (M-0332) of the Chinese-German Research Center of the National Science Foundation of China (NSFC) and the German Research Council (DFG), the China Postdoctoral Science Foundation (Certificate Number: 2023M741464), and the Jiangsu Funding Program for Excellent Postdoctoral Talent (2023ZB018).

## Declaration of competing interest

The authors declare no competing interests.

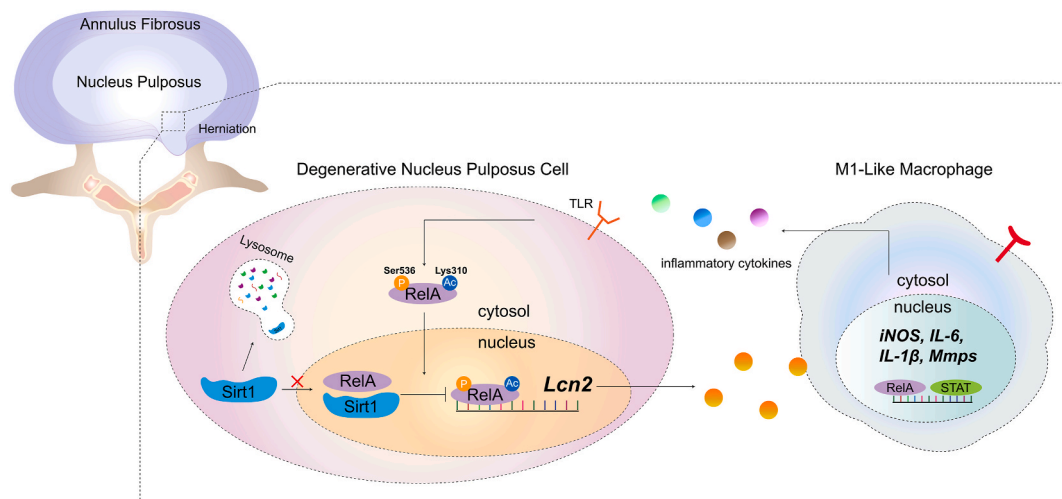


**Fig. 8.** Schematic diagram of the mechanism by which Sirt1 deficiency aggravates macrophage inflammatory response via NF- $\kappa$ B/*Lcn2* axis in IVDD. During aging and intervertebral disc degeneration, Sirt1 protein undergoes autophagic degradation within the lysosome. Sirt1 deficiency leads to the acetylation of lysine 310 on RelA, thereby enhancing its activity and triggering the NF- $\kappa$ B/*Lcn2* axis. This, in turn, promotes macrophages recruitment and M1 polarization, continuously exacerbating the chronic inflammatory microenvironment of intervertebral disc and ultimately destabilizing the homeostasis of nucleus pulposus.

## Appendix A. Supplementary data

Supplementary data to this article can be found online at <https://doi.org/10.1016/j.jot.2024.11.008>.

## References

- [1] Disease GBD, Injury I, Prevalence C. Global, regional, and national incidence, prevalence, and years lived with disability for 354 diseases and injuries for 195 countries and territories, 1990–2017: a systematic analysis for the Global Burden of Disease Study 2017. *Lancet* 2018;392(10159):1789–858.
- [2] Walker BF. The prevalence of low back pain: a systematic review of the literature from 1966 to 1998. *J Spinal Disord* 2000;13(3):205–17.
- [3] Shamji MF, Setton LA, Jarvis W, So S, Chen J, Jing L, et al. Proinflammatory cytokine expression profile in degenerated and herniated human intervertebral disc tissues. *Arthritis Rheum* 2010;62(7):1974–82.
- [4] Yamamoto J, Maeno K, Takada T, Kakutani K, Yurube T, Zhang Z, et al. Fas ligand plays an important role for the production of pro-inflammatory cytokines in intervertebral disc nucleus pulposus cells. *J Orthop Res* 2013;31(4):608–15.
- [5] Madhu V, Guntur AR, Risbud MV. Role of autophagy in intervertebral disc and cartilage function: implications in health and disease. *Matrix Biol* 2021;100–101:207–20.
- [6] Ni L, Zheng Y, Gong T, Xiu C, Li K, Sajilafu, et al. Proinflammatory macrophages promote degenerative phenotypes in rat nucleus pulposus cells partly through ERK and JNK signaling. *J Cell Physiol* 2019;234(5):5362–71.
- [7] Patil P, Dong Q, Wang D, Chang J, Wiley C, Demaria M, et al. Systemic clearance of p16(INK4a)-positive senescent cells mitigates age-associated intervertebral disc degeneration. *Aging Cell* 2019;18(3):e12927.
- [8] Yang S, Zhang F, Ma J, Ding W. Intervertebral disc ageing and degeneration: the antiapoptotic effect of oestrogen. *Ageing Res Rev* 2020;57:100978.
- [9] Vaziri H, Dessain SK, Ng Eaton E, Imai SI, Frye RA, Pandita TK, et al. hSIRT1(SIRT1) functions as a NAD-dependent p53 deacetylase. *Cell* 2001;107(2):149–59.
- [10] Brunet A, Sweeney LB, Sturgill JF, Chua KF, Greer PL, Lin Y, et al. Stress-dependent regulation of FOXO transcription factors by the SIRT1 deacetylase. *Science* 2004;303(5666):2011–5.
- [11] Yeung F, Hoberg JE, Ramsey CS, Keller MD, Jones DR, Frye RA, et al. Modulation of NF-kappaB-dependent transcription and cell survival by the SIRT1 deacetylase. *EMBO J* 2004;23(12):2369–80.
- [12] Picard F, Kurtev M, Chung N, Toprak-Ngarm A, Senawong T, Machado De Oliveira R, et al. Sirt1 promotes fat mobilization in white adipocytes by repressing PPAR-gamma. *Nature* 2004;429(6993):771–6.
- [13] Che H, Li J, Li Y, Ma C, Liu H, Qin J, et al. p16 deficiency attenuates intervertebral disc degeneration by adjusting oxidative stress and nucleus pulposus cell cycle. *Elife* 2020;9.
- [14] Ji ML, Jiang H, Zhang XJ, Shi PL, Li C, Wu H, et al. Preclinical development of a microRNA-based therapy for intervertebral disc degeneration. *Nat Commun* 2018;9(1):5051.
- [15] Zhou N, Lin X, Dong W, Huang W, Jiang W, Lin L, et al. SIRT1 alleviates senescence of degenerative human intervertebral disc cartilage endo-plate cells via the p53/p21 pathway. *Sci Rep* 2016;6:22628.
- [16] Yi W, Wen Y, Tan F, Liu X, Lan H, Ye H, et al. Impact of NF-kappaB pathway on the apoptosis-inflammation-autophagy crosstalk in human degenerative nucleus pulposus cells. *Aging (Albany NY)* 2019;11(17):7294–306.
- [17] Mosialou I, Shikhel S, Liu JM, Maurizi A, Luo N, He Z, et al. MC4R-dependent suppression of appetite by bone-derived lipocalin 2. *Nature* 2017;543(7645):385–90.
- [18] Xiao X, Yeoh BS, Vijay-Kumar M. Lipocalin 2: an emerging player in iron homeostasis and inflammation. *Annu Rev Nutr* 2017;37:103–30.
- [19] Rathore KI, Berard JL, Redensek A, Chierzi S, Lopez-Vales R, Santos M, et al. Lipocalin 2 plays an immunomodulatory role and has detrimental effects after spinal cord injury. *J Neurosci* 2011;31(38):13412–9.
- [20] Griffith JF, Wang YX, Antonio GE, Choi KC, Yu A, Ahuja AT, et al. Modified Pfirrmann grading system for lumbar intervertebral disc degeneration. *Spine* 2007;32(24):E708–12.
- [21] Jiang T, Qin T, Gao P, Tao Z, Wang X, Wu M, et al. SIRT1 attenuates blood-spinal cord barrier disruption after spinal cord injury by deacetylating p66Shc. *Redox Biol* 2023;60:102615.
- [22] Ma C, Qi X, Wei YF, Li Z, Zhang HL, Li H, et al. Amelioration of ligamentum flavum hypertrophy using umbilical cord mesenchymal stromal cell-derived extracellular vesicles. *Bioact Mater* 2023;19:139–54.
- [23] Gu X, Gu B, Lv X, Yu Z, Wang R, Zhou X, et al. 1, 25-dihydroxy-vitamin D3 with tumor necrosis factor-alpha protects against rheumatoid arthritis by promoting p53 acetylation-mediated apoptosis via Sirt1 in synoviocytes. *Cell Death Dis* 2016;7(10):e2423.
- [24] Ma C, Liu H, Wei Y, Li H, Miao D, Ren Y. Exogenous PTH 1-34 attenuates impaired fracture healing in endogenous PTH deficiency mice via activating Indian hedgehog signaling pathway and accelerating endochondral ossification. *Front Cell Dev Biol* 2021;9:750878.
- [25] Li Y, Wei Y, Li H, Che H, Miao D, Ma C, et al. Exogenous parathyroid hormone alleviates intervertebral disc degeneration through the sonic hedgehog signalling pathway mediated by CREB. *Oxid Med Cell Longev* 2022;2022:9955677.
- [26] Sun W, Qiao W, Zhou B, Hu Z, Yan Q, Wu J, et al. Overexpression of Sirt1 in mesenchymal stem cells protects against bone loss in mice by FOXO3a deacetylation and oxidative stress inhibition. *Metabolism* 2018;88:61–71.
- [27] Boos N, Weissbach S, Rohrbach H, Weiler C, Spratt KF, Nerlich AG. Classification of age-related changes in lumbar intervertebral discs: 2002 Volvo Award in basic science. *Spine* 2002;27(23):2631–44.
- [28] Latimer M, Ernst MK, Dunn LL, Drutsakaya M, Rice NR. The N-terminal domain of IkkappaB alpha masks the nuclear localization signal(s) of p50 and c-Rel homodimers. *Mol Cell Biol* 1998;18(5):2640–9.
- [29] Fournier DE, Kiser PK, Shoemaker JK, Battie MC, Seguin CA. Vascularization of the human intervertebral disc: a scoping review. *JOR Spine* 2020;3(4):e1123.
- [30] Xiao L, Hu B, Ding B, Zhao Q, Liu C, Oner FC, et al. N(6)-methyladenosine RNA methyltransferase like 3 inhibits extracellular matrix synthesis of endplate chondrocytes by downregulating sex-determining region Y-Box transcription factor 9 expression under tension. *Osteoarthritis Cartilage* 2022;30(4):613–25.
- [31] Che H, Ma C, Li H, Yu F, Wei Y, Chen H, et al. Rebalance of the polyamine metabolism suppresses oxidative stress and delays senescence in nucleus pulposus cells. *Oxid Med Cell Longev* 2022;2022:8033353.
- [32] Lyu FJ, Cui H, Pan H, Mc Cheung K, Cao X, Iatridis JC, et al. Painful intervertebral disc degeneration and inflammation: from laboratory evidence to clinical interventions. *Bone Res* 2021;9(1):7.
- [33] Yamagishi A, Nakajima H, Kokubo Y, Yamamoto Y, Matsumine A. Polarization of infiltrating macrophages in the outer annulus fibrosus layer associated with the process of intervertebral disc degeneration and neural ingrowth in the human cervical spine. *Spine J* 2022;22(5):877–86.
- [34] Saunders AN. Incubator noise: a method to decrease decibels. *Pediatr Nurs* 1995;21(3):265–8.
- [35] Wang Y, Wang H, Zhuo Y, Hu Y, Zhang Z, Ye J, et al. SIRT1 alleviates high-magnitude compression-induced senescence in nucleus pulposus cells via PINK1-dependent mitophagy. *Aging (Albany NY)* 2020;12(16):16126–41.
- [36] Woertgen C, Rothoerl RD, Brawanski A. Influence of macrophage infiltration of herniated lumbar disc tissue on outcome after lumbar disc surgery. *Spine* 2000;25(7):871–5.
- [37] Risbud MV, Shapiro IM. Role of cytokines in intervertebral disc degeneration: pain and disc content. *Nat Rev Rheumatol* 2014;10(1):44–56.
- [38] Xu C, Wang L, Fozouni P, Evjen G, Chandra V, Jiang J, et al. SIRT1 is downregulated by autophagy in senescence and ageing. *Nat Cell Biol* 2020;22(10):1170–9.
- [39] Mima Y, Suzuki S, Fujii T, Morikawa T, Tamaki S, Takubo K, et al. Potential involvement of semaphorin 3A in maintaining intervertebral disc tissue homeostasis. *J Orthop Res* 2019;37(4):972–80.
- [40] Chen F, Jiang H, Liu H, Li Z, Pei Y, Wang H, et al. Melatonin alleviates intervertebral disc degeneration by disrupting the IL-1beta/NF-kappaB-NLRP3 inflammasome positive feedback loop. *Bone Res* 2020;8:10.
- [41] Shen J, Fang J, Hao J, Zhong X, Wang D, Ren H, et al. SIRT1 inhibits the catabolic effect of IL-1beta through TLR2/SIRT1/NF-kappaB pathway in human degenerative nucleus pulposus cells. *Pain Physician* 2016;19(1):E215–26.
- [42] Narita T, Weinert BT, Choudhary C. Functions and mechanisms of non-histone protein acetylation. *Nat Rev Mol Cell Biol* 2019;20(3):156–74.
- [43] Yang XJ, Seto E. Lysine acetylation: codified crosstalk with other posttranslational modifications. *Mol Cell* 2008;31(4):449–61.
- [44] Matsuzaki H, Daitoku H, Hatta M, Aoyama H, Yoshimochi K, Fukamizu A. Acetylation of Foxo1 alters its DNA-binding ability and sensitivity to phosphorylation. *Proc Natl Acad Sci U S A* 2005;102(32):11278–83.
- [45] Westergaard M, Henningsen J, Johansen C, Rasmussen S, Svendsen ML, Jensen UB, et al. Expression and localization of peroxisome proliferator-activated receptors and nuclear factor kappaB in normal and lesional psoriatic skin. *J Invest Dermatol* 2003;121(5):1104–17.
- [46] Yang M, Wu X, Li L, Li S, Li N, Mao M, et al. COMM10 inhibits tumor progression and induces apoptosis by blocking NF-kappaB signal and values up BCLC staging in predicting overall survival in hepatocellular carcinoma. *Clin Transl Med* 2021;11(5):e403.
- [47] Conde J, Lazzaro V, Scotece M, Abella V, Villar R, Lopez V, et al. Corticoids synergize with IL-1 in the induction of LCN2. *Osteoarthritis Cartilage* 2017;25(7):1172–8.
- [48] Ye D, Yang K, Zang S, Lin Z, Chau HT, Wang Y, et al. Lipocalin-2 mediates non-alcoholic steatohepatitis by promoting neutrophil-macrophage crosstalk via the induction of CXCR2. *J Hepatol* 2016;65(5):988–97.
- [49] Yamamoto Y, Kokubo Y, Nakajima H, Honjoh K, Watanabe S, Matsumine A. Distribution and polarization of hematogenous macrophages associated with the progression of intervertebral disc degeneration. *Spine* 2022;47(4):E149–58 (Phila Pa 1976).
- [50] Nakazawa KR, Walter BA, Laudier DM, Krishnamoorthy D, Mosley GE, Spiller KL, et al. Accumulation and localization of macrophage phenotypes with human intervertebral disc degeneration. *Spine J* 2018;18(2):343–56.
- [51] Wang Q, Li S, Tang X, Liang L, Wang F, Du H. Lipocalin 2 protects against *Escherichia coli* infection by modulating neutrophil and macrophage function. *Front Immunol* 2019;10:2594.